Original Article

Intelligent Wireless Endoscopic Image Classification using Gannet Optimization with Deep Learning Model

M. Amirthalingam[1], R. Ponnusamy[2]

[1,2]*Department of Computer and Information Science, Annamalai University, Annamalai Nagar*

[1]*Corresponding Author : amir.cdm@gmail.com*

Abstract - Wireless capsule endoscopy (WCE) is a non-invasive wireless imaging technology that gained wider popularity. The main drawback of WCE is that it produces a massive amount of images that healthcare professionals should analyze, which is time-consuming. Many researchers have suggested machine learning and image-processing methods for classifying gastrointestinal tract disorders. Data augmentation and classical image processing techniques are integrated with the adjustable pre-trained deep convolutional neural network (DCNN) to categorize diseases in the digestive tract from WCE images. This study develops an Intelligent Wireless Endoscopic Image Classification using Gannet Optimization Algorithm with Deep Learning (IWEIC-GOADL) model. The IWEIC-GOADL technique mainly examines the WCE images for classification purposes. As a preprocessing step, the presented IWEIC-GOADL technique executes the Gabor filtering (GF) method for the noise removal process. In addition, the presented IWEIC-GOADL technique employs a deconvolution VGG19 (DeVGG19) model for feature vector generation, and its hyperparameter tuning process takes place by the GOA. Finally, the IWEIC-GODL technique applies the deep belief network (DBN) model for WCE image classification purposes. A wide range of simulations was performed on a benchmark dataset to demonstrate the better performance of the IWEIC-GODL technique. The stimulation outcome stated the improvements of the IWEIC-GODL algorithm over other recent techniques.

Keywords - Medical imaging, Computer vision, Wireless capsule endoscopy, Deep learning, Gannet optimization algorithm.

1. Introduction

Wireless capsule endoscopy (WCE) can be defined as a non-invasive, wireless imaging gadget that has advanced quickly in the past few years [1]. The medical analysis, including the utility of WCE, is executed in a hospital or ambulatory setup on an outpatient basis. The patient devours a small tablet after fasting overnight (8 to 12 hours) [2]. That pill was fitted with a wireless circuit and micro-imaging video technology for the transmission and acquisition of imageries. The mechanism even involves software that offers localization of the gadgets on their way through the intestine [3]. While moving, imageries were captured at a frame rate of two frames per second (fps) if the newest prototype of WCE generated using PillCam SB 3 tablet can obtain at a frame rate of two to six fps depending on pill speed since it travelled over the SB [4]. Such images were sent to a data recorder, and almost 8 hours later ingestion, the victim returned to the hospital, where imageries and data were taken. The pill was passed into the stools of patients in 24 to 48 hours [29].

WCE was regarded as a first-line inspection tool that finds various kinds of abnormality, which includes bleeding [6-8], Crohn's disease, polyps, and ulcers. A single scan may add millions of GI tract images for all patients. However, only a few pieces of evidence of abnormality may appear. Hence, identifying bleeding areas in WCE images was a tedious and time-taking task for doctors, which may include several difficulties, including low contrast and complicated background, differences in colour and lesion, thus affecting the performance of subsequent classification and segmentation [9]. Such problems complicate objective disease detection requiring the ideas of many specialists to evade inaccurate detection. Computer-Aided abnormality identification in capsule endoscopy imageries has unlocked areas of research in the field of Machine Learning (ML) and medical image processing [10]. To detect and identify abnormality presented with distinct texture and colour paradigms, various techniques like image processing, deep learning (DL), and ML were leveraged [11, 12]. The accomplishment of the ML-related techniques relies on the aspects that can be utilized for indicating the anomalies and the techniques leveraged for extracting the features from images. DL methods use labelled datasets for learning features for identifying abnormalities [13-15].

This study develops an Intelligent Wireless Endoscopic Image Classification using Gannet Optimization Algorithm

with Deep Learning (IWEIC-GOADL) model. The presented IWEIC-GOADL technique executes the Gabor filtering (GF) method for the noise removal process. In addition, the presented IWEIC-GOADL technique employs a deconvolution VGG19 (DeVGG19) model for feature vector generation, and its hyperparameter tuning process takes place by the GOA. Finally, the IWEIC-GODL technique applies the deep belief network (DBN) model for WCE image classification. A wide range of simulations was performed on a standard dataset to demonstrate the better accomplishment of the IWEIC-GODL technique.

2. Related Works

In [16], the authors devised a novel computer-assisted diagnosis (CAD) method for detecting abnormalities in WCE images. After the preprocessing step, the descriptor given to a kernel ELM for performing the classifying procedure can be extracted by the author from these images. The descriptor utilized in this study was an integration among the HOG that was extracted with the use of a modified rotation-invariant LBP and hue element of the HSV colour space. Alaskar et al. [17] devise an automatic mechanism for classifying and detecting ulcers in WCE imageries related to existing DL networks. DL methods, and to be specific, CNNs, have newly become common in the recognition and analysis of medical images. In this study, 2 milestone CNN structures, one the GoogLeNet and one AlexNet, are widely assessed in object classification into non-ulcer or ulcer. Additionally, the author analyzes and examines the images detected as comprising ulcer objects to assess the used CNN's efficacy.

Son et al. [30] developed an automatic small bowel identification approach from prolonged uncut videos taken from WCE. Hereby, the colon and stomach are even distinguished. The presented approach depended on a CNN having temporal filtering on the predictive probability from the CNNs. The author employed the ResNet50 methodology for classifying 3 organs which include the stomach, colon, and small bowel. Marin-Santos et al. [19] devised a CNN to classify the CE images to find the affected lesions. The structure to solve this image classifier problem study was custom designed. This enabled various models to be made by enriching their accuracy and processing speed performance compared to other DL-related reference structures.

In [20], a deep CNN-related method, 'WCENet', was introduced for localization and anomaly detection (AD) in WCE imageries. The model functions in 2 stages. In the initial stage, a potential and simple attention-related alleviated CNN technique an image into one of the following 4 types: inflammatory, normal, polyp, vascular, or the image can be categorized in one of the anomalous classifications. It proceeded to the next stage for the localization anomalies. Vani and Prashanth [27] presented deep CNN for automated discernment of ulcers on various ratios of

amplified data that range from 1K to 10 K WCE images containing non-ulcer and ulcer imageries. A brief study of network structure for many techniques and depth can be executed.

3. The Proposed Model

In this study, a novel IWEIC-GOADL procedure has been introduced for WCE image categorization. The presented IWEIC-GOADL technique encompasses a GOA-based hyperparameter optimizer, GF preprocessing, DeVGG19 feature extraction, and DBN-based classification. In the presented IWEIC-GOADL technique, the GOA is applied as a hyperparameter optimizer, enhancing the overall WCI classification performance. Fig. 1 defines the comprehensive flow of the IWEIC-GOADL approach.
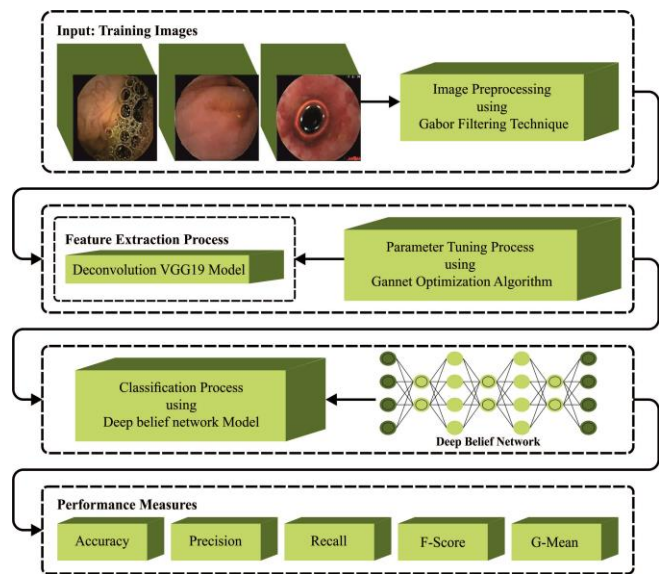
Fig. 1 Overall flow of the IWEIC-GOADL approach

3.1. Image Preprocessing

Firstly, the IWEIC-GOADL approach executes the GF method for the noise removal process. Gabor filtering (GF) was exploited in the projected method to higher the ridges and relax the valleys with the execution of short-term Fourier transformation comprising the Gaussian window from the spatial domain [22]. It supports obtaining deviation in textures and features from the fingerprint images to various orientations and scales. At the same time, the statistical feature created image features which are considerably accentuated by exploiting the frequency data and orientation from the fingerprint images by fine-tuning GF. A group of GF has been utilized on image $I(x, y)$ in different frequencies containing various orientations exploiting Gabor function $g(x, y)$ as written in Eq. (1).

$$g(x, y) = \exp\left(-\frac{x'^2 + \gamma^2 y'^2}{2\sigma^2}\right) \cos\left(2\pi \frac{X'}{l} + \phi\right) \quad (1)$$

At this point, $\chi' = xcox\theta + ys\dot{m}\theta$ and $y' = ycox\theta - xs\dot{m}\theta$. This Gabor transform is executed in the Gaussian envelope σ along with χ and y directions.

3.2. Feature Extraction using DeVGG19

For feature vector generation, the DeVGG19 model is used. Karen Simonian and Andrew designed a VGGNet, which is a CNN model [23]. By substituting the larger convolutional kernel of 5x5 and 11x11 sizes with the kernel of 3x3 size one by one, they found in VGGNet that the smaller convolutional kernel increases the depth of nonlinear network and makes the network increasingly difficult and capable of learning increasingly complex feature. It shows that the intensification in network depth could improve the accomplishment. However, the deep network needs massive computation requirements. VGG19 comprises various convolutional kernels which calculate various feature maps. The steel surface defect's feature map is achieved by convolving the input with the learned kernel, and later the non-linear activation function (ReLU) is applied to the convolved result. The new feature map can be attained with the aid of multiple kernels. The single feature value V in the feature maps is mathematically expressed as follows:

$$V = f\left(\sum_{i=1}^{n} p_i w_i + b\right) = f\left((w_1, w_2 \ldots w_n)\begin{pmatrix} p_1 \\ p_2 \\ \ldots \\ p_n \end{pmatrix} + b\right)$$
$$= f(W^T P + b) \qquad (2)$$

In Eq. (1), W and b denote the weight and bias value correspondingly, p indicates the input vectors and the kernel w is shared. Where $p = (p_1, p_2 \ldots p_i \ldots p_n)$ weight sharing method making the network easy for training and decreasing the model parameters. The activation function f presents non-linearity to CNN that helps multilayer networks to identify non-linear features. DeVGG19 is a deconvolution NN with a similar structure to the VGG19 model. The DeVGG19 network is established based on Unpooling and deconvolution modules, ReLU and Deconvolution. The feature in the convolutional kernels of every convolution layer is extracted and given into the pixel space for visualization. The DeVGG19 process is given below:

3.2.1. Filtering

The learned filter in the VGG19 can be applied for convolving the steel surface defect feature map of the preceding layers. Rather than the output of the lower layer, the similar transpose filters in DeVGG19 are only utilized for the modified feature maps to reverse these steps. These operations represent flipping every filter vertically and horizontally.

3.2.2. Unpooling

It is not possible to flip the operation of convolution networks; however, it is capable of selecting the proper location in the complex value in the maximal pooling function. Unpooling is applied in the DeVGG19 network to find the appropriate position for the variable changed from the upper layer, to maintain structural activation and form the refining steel surface defect results.

3.2.3. Rectification

In DeVGG19 or convent, the ReLu non-linearity can still be positive in the feature maps. Hence, using the similar ReLu function to make the feature maps positive and attain the defect feature reconstruction at all the layers.

This new feature image of the convolutional layer is mapped back to the input pixel using the three important steps. Moreover, demonstrate the outcome of the steel surface defect feature image eventually.

3.3. Hyperparameter Tuning using GOA

In this work, the GOA is applied as a hyperparameter optimizer. The GOA mimics a procedure of Gannet in a lake which aims at nourishing it [28]. The Gannet is a huge waterfowl better suited for feeding on target in the water because of its magnitude. It is capable of grabbing objectives and bringing them back at a quicker rate during the feeding procedure. The fish line up or food on them in semicircles if the flocks of gannets determine schools of fish.

The GOA takes 2 stages of development and exploration. An initial initializing of GOA is for determining a group of random solutions x_{id} representing n D-dimension Gannet's places of n^*D matrices to begin with, and the optimum solution reached in these matrices is assumed as a global better solution. The equation to attain the solution of matrices is given below:

$$x_{id} = r_0(ub_d - lb_d) + lb_{d'} i = 1,2,\ldots,N, d = 1,2,\ldots,Dim \quad (3)$$

In Eq. (3), N implies the entire count of gannets. Dim signifies the upper limit of the dimensional of the solutions. ub_d and lb_d determines the upper and lower limits of every dimension. r_0 refers to the random number from zero to one. Afterwards, the initialisation of GOA was accomplished, and Gannets began with the hunt. During this exploration stage, Gannets takes 2 dive modes: U-shaped dive that is appropriate to feed on fish in shallow water and matches Eq. (6). Then, V-shaped dive that is appropriate to feed on fish in deep water, equivalent to Eq. (7),

$$t = 1 - \frac{It_k}{K_{\max}}, k = 1,2,\ldots,K_{\max} \qquad (4)$$

$$a_u = 2cos(2\pi r_1) \times t \qquad (5)$$

$$b_v = 2V(2\pi r_2) \times t \qquad (6)$$

$$V_{sh}(y) = \begin{cases} -\dfrac{y}{\pi} + 1 & y \in (0, \pi) \\ \dfrac{y}{\pi} - 1 & y \in (\pi, 2\pi) \end{cases} \quad (7)$$

Whereas It_k represents the kth iteration and K_{max} signifies the upper boundary of the count of iterations, r_1 denotes the random number from zero to one, like r_2.

The probability of selecting these dive approaches is similar; thus, q random number was determined to represent the random selection of hunting approaches. The updating position formula is given below,

$$MX_i(t + 1) = \begin{cases} u_1 + u_2 + X_j(t) & q \geq 0.5(a) \\ v_1 + v_2 + X_j(t) & q < 0.5(b) \end{cases} \quad (8)$$

$$u_2 = A\left(X_j(t) - X_{rand}(t)\right) \quad (9)$$

$$v_2 = B\left(X_i(t) - X_{Mean}(t)\right) \quad (10)$$

$$A = (2r_3 - 1)a_u \quad (11)$$

$$B = (2r_4 - 1)b_v \quad (12)$$

Whereas r_3 and r_4 both range in a random integer between zero and one, u_1 ranges in $-a_u$ and a_u, and v_1 ranges in $-b_v$ and b_v. The ith the solution from the population was represented by $X_i(t)$. $X_{rand}(t)$ exemplifies the random selection of solutions in the whole population, $X_{Mean}(t)$ denotes the solution at the centre of populations, and $X_{Mean}(t)$ was computed as illustrated in Eq. (13),

$$X_{Mean}(t) = \frac{1}{N}\sum_{i=1}^{N} X_i(t) \quad (13)$$

In this exploitation step, fish should take two actions for further development if the Gannet encounters fish that suddenly turn around as follows:

$$Capturability = \frac{1}{Rt_2} \quad (14)$$

$$t_2 = 1 + \frac{It_k}{K_{max}} \quad (15)$$

$$R = \frac{Mv^2}{L} \quad (16)$$

$$L = 0.2 + (2 - 0.2)r_5 \quad (17)$$

Where $M = 2.5$ kg is set as per the average mass of the Gannet population, r_5 characterizes a randomly generated value within [0,1], and $v = 1.5 m/s$ signifies the rate of Gannet in the water. Once the fish escapes and the position

where the fish escape is within the capture ability of the Gannet, making the location be changed as it chases the fish; or else, the Gannet lose the goal and takes the Levy flight for location updating to study the next target χ at random, with the updating location equation given as follows:

$$MX_i(It + 1) =$$
$$\begin{cases} X_i(It) + t \times Delt \times (X_i(It) - X_{besi}(It)) & Capturability \geq c(a) \\ X_{best}(It) - (X_{best}(It) - X_{besi}(It)) \times t \times Lv & Capturability < c(b) \end{cases} \quad (18)$$

$$Delt = Capturability \times |X_i(It) - X_{Best}(It)| \quad (19)$$

$$Lv = Levy(Dim) \quad (20)$$

Where c denotes the constant value set to 0.2. X_{besi} (It) indicates the optimum Gannet as follows:

Algorithm 1: GOA

$\overline{Input: N_p}$: Population size; $\cdot K_{max}$: The upper boundary of the number of iterations;$\cdot Dim$: problem dimension,
Output: Fitness value; Global optimum location in the population;
Initializing the location of every Gannet in the population.
Produce a location matrix MX_j according to every initialized Gannet location and
Compute the fitness values for all the Gannets.
For $It_k < K_{max}$ do
If $rand \geq 0.5$ then
    For MX_i do
        If $rand \geq 0.5$ then
Upgrade Gannet X_i)
            Else
Upgrade Gannet X_i
              End
           End
        Else
      For MX_i do
        If $c \geq 0.2$ then
           Upgrade Gannet X_i
        Else
           Upgrade Gannet X_i
        End
      End
End
For MX_i do
Compute the fitness value of every Gannet X_i in MX_i;
Upgrade MX_i by using X_i fitness;
End
End

$$Levy(Dim) = 0.01\frac{\mu\sigma}{|v|^{\frac{1}{\beta}}} \quad (21)$$

$$\sigma = \left(\frac{\sin\left(\frac{\pi\beta}{2}\right)\Gamma(1 + \beta)}{\Gamma\left(\frac{1 + \beta}{2}\right)\beta 2\left(\frac{\beta - 1}{2}\right)}\right)^{\frac{1}{\beta}} \quad (22)$$

Where μ and σ denote the randomly generated value within [0,1], and β denotes the predefined constant with the value of 1.5.

The abovementioned equation is used to update the location of Gannet in the course of predation. Algorithm 1 demonstrates the pseudocode of GOA:

Fitness choice is a critical aspect of the GOA system. The solution encoder was utilized to assess the aptitude (goodness) of candidate results. At present, the precision value is the key factor employed to plan a fitness function.

$$Fitness = \max(P) \tag{23}$$

$$P = \frac{TP}{TP + FP} \tag{24}$$

In which TP stands for the true positive, and FP determines the false positive value.

3.4. Image Classification using DBN

Finally, the DBN model is exploited for the WCE image classification process. DBN is based on the DNN with a great count of hidden units and multiple hidden layers (HLs) [24, 25]. Fig. 2 represents the framework of DBN. Usually, the DBN was related to the RBM scheme, viz., collected from the resulting layer. Likewise, the DBN utilizes supervised fine-tuning techniques to change the method by labelled datasets and a greedy unsupervised learning approach to train RMB. The RBM comprises the visible layer (v) and hidden layer (h) and is related to undirected weighted. HL of RBM was assumed as a visible layer of future RBM to stack RBMs in DBN. The variable set of RMB as $= (w, b, a)$, whereas w_{ij} suggests the weighted among v_i and h_j. b_i and a_j indicates the layer bias. The RBM determined equal energy was demonstrated as:

$$E(v, h|\theta) = -\sum_i b_i v_i - \sum_j a_j h_j - \sum_i \sum_j w_{ij} v_i h_j \tag{25}$$

The joint likelihood distribution of hidden and visible layers is determined by:

$$p(v, h|\theta) = \frac{\exp\left(-E(v, h|\theta)\right)}{\sum_{v,h} \exp\left(-E(v, h|\theta)\right)} \tag{26}$$

But marginal likelihood distribution of visible layer is written by:

$$p(v|\theta) = \frac{\sum_h \exp\left(-E(v, h|\theta)\right)}{\sum_{v,h} \exp\left(-E(v, h|\theta)\right)}. \tag{27}$$

For obtaining a best θ value to single data vector v, the gradient of log probability was estimated dependent upon the employed function,

$$\frac{\partial logp(v|\theta)}{\partial w_{ij}} = \langle v_i h_j \rangle_{data} - \langle v_i h_j \rangle_{model},$$

$$\frac{\partial logp(v|\theta)}{\partial a_j} = \langle h_j \rangle_{data} - \langle h_j \rangle_{model}, \tag{28}$$

$$\frac{\partial logp(v|\theta)}{\partial b_i} = \langle v_i \rangle_{data} - \langle v_i \rangle_{model},$$

But $\langle \cdot \rangle$ implies the expectation by the dispersion of exact subscript. Due to the lack of interactions among units in identical layers, $\langle \cdot \rangle_{data}$ represents the simply accomplished by estimating the conditional likelihood distribution as:

$$p(h_j|v, \theta) = \frac{1}{1 + \exp\left(-\sum_i w_{ij} v_i - a_j\right)}, \tag{29}$$

$$p(v_i|h, \theta) = \frac{1}{1 + \exp\left(-\sum_j w_{ij} h_j - b_i\right)}.$$

The sigmoid function represents the activation function. If there should be $\langle \cdot \rangle_{model}$, Contrastive Divergence (CD) learning element was executed by reconstruction model to decrease the difference of 2 Kullback-Leibler divergences (KL). Primarily, CD learning was more effective in actual application and restricted the process costs than the Gibbs sampling approach. Therefore, the weights in the DBN layer endure trained with an unlabelled dataset by a greedy and fast unsupervised approach. On the chance of predictive, a supervised layer has been involved in DBN to change the learned aspects using labelled data from the application of an up-down fine-tune system. At present, the Fully Connected (FC) layer performs as the topmost layer.
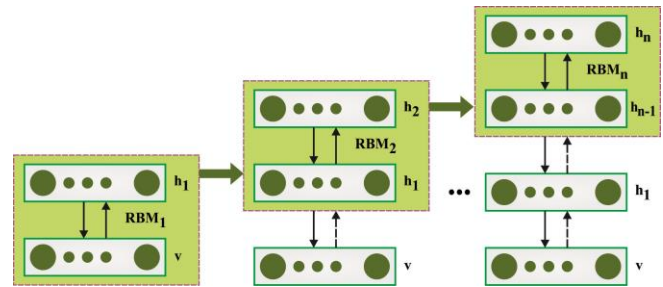
Fig. 2 DBN structure

4. Experimental Validation

In this section, the experimental WCI image classification outcomes of the IWEIC-GOADL system are inspected on the database containing 300 WCE images, as represented in Table 1.

Table 1. Dataset details

Class Name	No. of Images
Normal	150
Infected	150
Total Number of Images	300
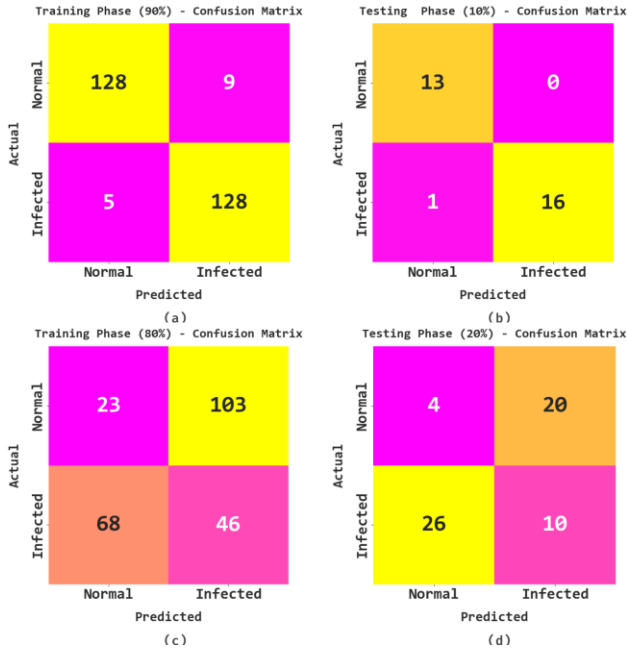
Fig. 3 Confusion matrices of IWEIC-GOADL approach (a-b) TRS/TSS of 90:10 and (c-d) TRS/TSS of 80:20

The confusion matrices of the IWEIC-GOADL approach are revealed in Fig. 3. The outcomes recognize that the IWEIC-GOADL protocol has properly analyzed the normal and infected trials. For samples with 90% of TRS, the IWEIC-GOADL procedure has identified 128 normal samples and 128 infected samples. Moreover, with 10% of TSS, the IWEIC-GOADL algorithm has identified 13 normal samples and 16 infected samples. Simultaneously, with 80% of TSS, the IWEIC-GOADL approach has identified 23 normal samples and 46 infected samples. Finally, with 20% of TSS, the IWEIC-GOADL system has identified 4 normal samples and 10 infected samples.

Table 2. WCE outcome of IWEIC-GOADL approach on TRS/TSS of 90:10

Class	Accuracy$_{bal}$	Precision	Recall	F-Score	G-Mean
Training Phase (90%)					
Normal	93.43	96.24	93.43	94.81	94.83
Infected	96.24	93.43	96.24	94.81	94.83
Average	**94.84**	**94.84**	**94.84**	**94.81**	**94.83**
Testing Phase (10%)					
Normal	100.00	92.86	100.00	96.30	97.01
Infected	94.12	100.00	94.12	96.97	97.01
Average	**97.06**	**96.43**	**97.06**	**96.63**	**97.01**

In Table 2 and Fig. 4, an overall WCE result analysis of the IWEIC-GOADL technique is assessed with 90% TRS and 10% TSS. The experimental results inferred that the IWEIC-GOADL technique has accurately categorized the normal and

infected trials. For instance, with 90% of TRS, the IWEIC-GOADL procedure gains average $accu_{bal}$, $prec_n$, $reca_l$, F_{score}, and G_{mean} of 94.84%, 94.84%, 94.84%, 94.81%, and 94.83% respectively. Meanwhile, with 10% of TSS, the IWEIC-GOADL approach attains average $accu_{bal}$, $prec_n$, $reca_l$, F_{score}, and G_{mean} of 97.06%, 96.43%, 97.06%, 96.63%, and 97.01% correspondingly.
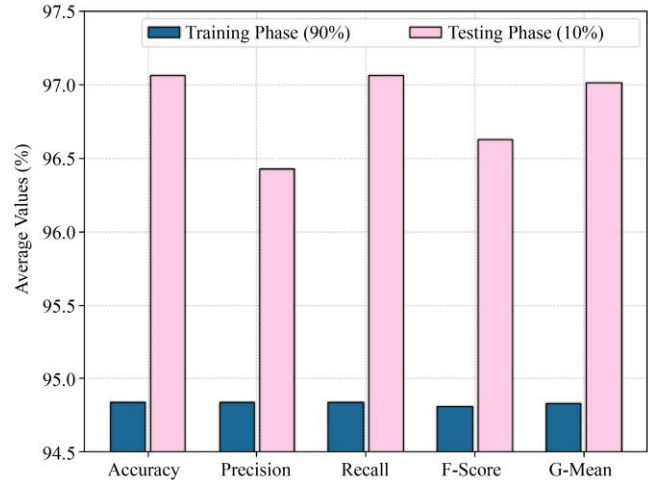
Fig. 4 Average outcome of IWEIC-GOADL approach on TRS/TSS of 90:10

In Table 3 and Fig. 5, an overall WCE outcome investigation of the IWEIC-GOADL approach is assessed with 80% of TRS and 20% of TSS. The experimental result stated that the IWEIC-GOADL algorithm accurately classified the normal and infected trials. For instance, with 80% of TRS, the IWEIC-GOADL system reaches average $accu_{bal}$, $prec_n$, $reca_l$, F_{score}, and G_{mean} of 99.13%, 99.21%, 99.13%, 99.16% and 99.13% correspondingly. In the meantime, with 10% of TSS, the IWEIC-GOADL algorithm obtains average $accu_{bal}$, $prec_n$, $reca_l$, F_{score}, and G_{mean} of 98.57%, 98.08%, 98.57%, 98.29% and 98.56% correspondingly.

Table 3. WCE outcome of IWEIC-GOADL approach on TRS/TSS of 80:20

Class	Accuracy$_{bal}$	Precision	Recall	F-Score	G-Mean
Training Phase (80%)					
Normal	98.26	100.00	98.26	99.12	99.13
Infected	100.00	98.43	100.00	99.21	99.13
Average	**99.13**	**99.21**	**99.13**	**99.16**	**99.13**
Testing Phase (20%)					
Normal	97.14	100.00	97.14	98.55	98.56
Infected	100.00	96.15	100.00	98.04	98.56
Average	**98.57**	**98.08**	**98.57**	**98.29**	**98.56**
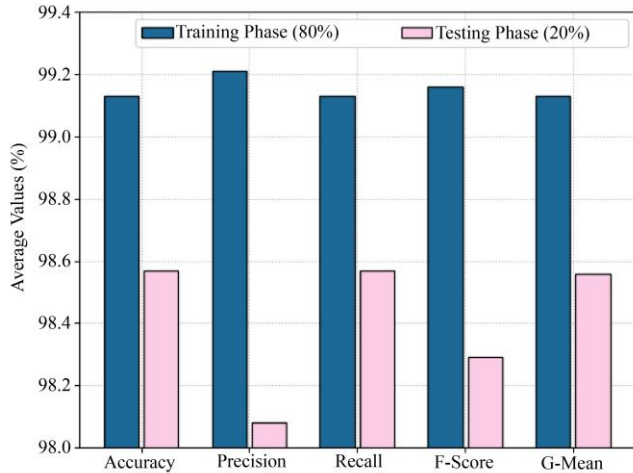
Fig. 5 Average outcome of IWEIC-GOADL approach on TRS/TSS of 80:20

The TACY and VACY of the IWEIC-GOADL algorithm are examined on WCE accomplishment in Fig. 6. The figure referred that the IWEIC-GOADL approach has exhibited higher accomplishment with maximal values of TACY and VACY. The IWEIC-GOADL approach has obtained higher TACY outcomes.

The TLOS and VLOS of the IWEIC-GOADL approach are tested on WCE accomplishment in Fig. 7. The figure implied that the IWEIC-GOADL methodology had demonstrated the best accomplishment with minimum values of TLOS and VLOS. The IWEIC-GOADL approach has resulted in lower VLOS results.
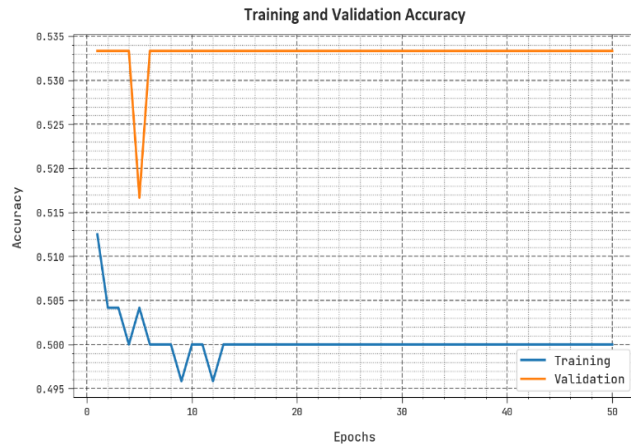
Fig. 6 TACY and VACY outcome of the IWEIC-GOADL approach

Evident precision-recall research of the IWEIC-GOADL algorithm in the test dataset is exposed in Fig. 8. The figure states that the IWEIC-GOADL methodology has an outcome in higher values of precision-recall values in two class labels. An elaborated ROC research of the IWEIC-GOADL approach in the test dataset is displayed in Fig. 9. The outcomes stated that the IWEIC-GOADL system had exhibited its capacity to categorize two class labels.
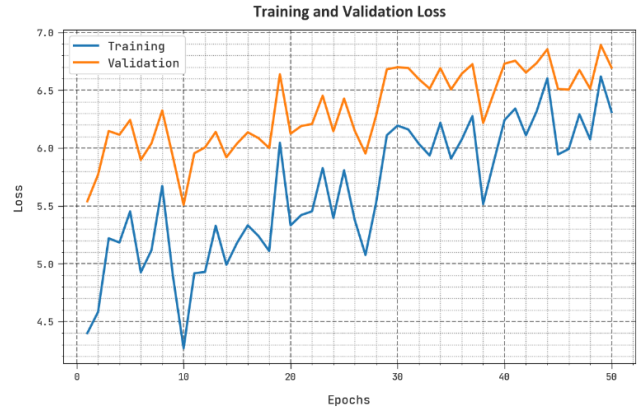
Fig. 7 TLOS and VLOS outcome of the IWEIC-GOADL approach
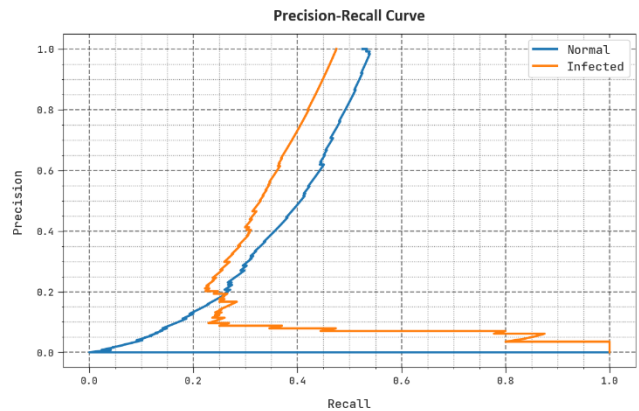
Fig. 8 Precision-recall outcome of the IWEIC-GOADL approach
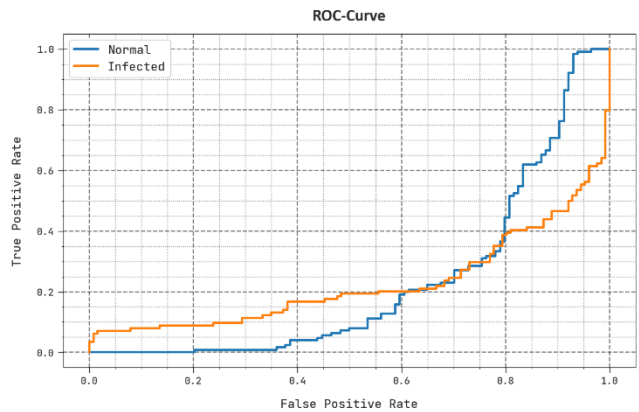
Fig. 9 ROC outcome of the IWEIC-GOADL approach

Table 4. Relative analysis of the IWEIC-GOADL algorithm with other prevailing systems

Methods	Accuracy	Precision	Recall	F1-Score
IWEIC-GOADL	99.13	99.21	99.13	99.16
RF Model	96.51	97.34	97.10	97.23
ETC Model	93.36	93.72	93.46	92.80
LR Model	87.46	90.50	88.49	88.36
SVM Model	89.31	91.08	88.78	88.77
DTC Model	90.60	92.57	91.62	91.06
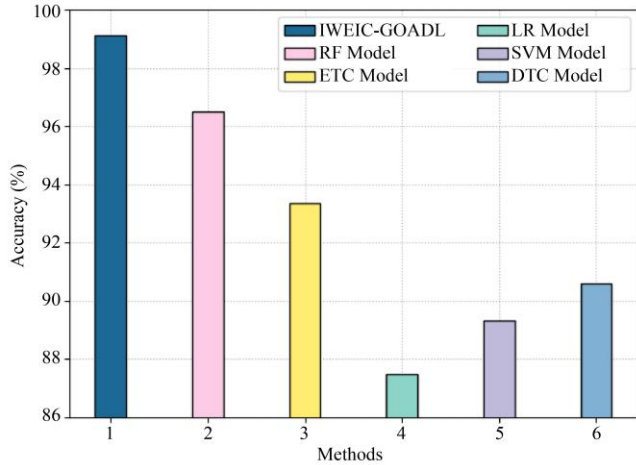
Fig. 10 $Accu_y$ analysis of the IWEIC-GOADL algorithm with other existing systems

In Table 4, the comparative results of the IWEIC-GOADL technique with recent models are well-studied. Fig. 10 exhibits a comparison study of the IWEIC-GOADL method with prevailing prototypes in terms of $accu_y$. The results indicate that the LR prototype demonstrates lower $accu_y$ of 87.46%. Then, the SVM and DTC models result in slightly closer $accu_y$ of 89.31% and 90.60%, respectively. Meanwhile, the ETC model accomplishes moderate $accu_y$ of 93.36%. Furthermore, the RF model reaches reasonable $accu_y$ of 96.51%. But the IWEIC-GOADL technique results in maximum $accu_y$ of 99.13%.

Fig. 11 exhibitions a comparative analysis of the IWEIC-GOADL method with existing systems in terms of $prec_n$. The outcomes indicate that the LR system exhibits lower $prec_n$ of 90.50%. Afterwards, the SVM and DTC models result in somewhat closer $prec_n$ of 91.08% and 92.57%, correspondingly. In the meantime, the ETC method achieves moderate $prec_n$ of 93.72%. Additionally, the RF approach reaches reasonable $prec_n$ of 97.34%. But the IWEIC-GOADL approach results in maximal $prec_n$ of 99.21%.
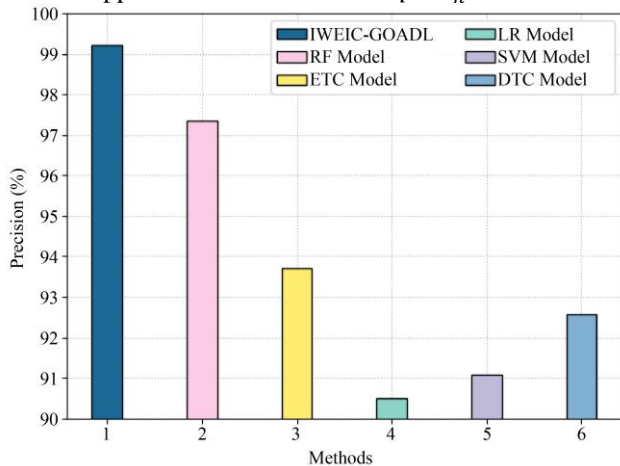
Fig. 11 $Prec_n$ analysis of the IWEIC-GOADL algorithm with other existing systems

Fig. 12 reveals a comparative investigation of the IWEIC-GOADL technique with existing approaches in terms of $reca_l$. The results indicate that the LR approach validates lesser $reca_l$ of 88.49%. In addition, the SVM and DTC models result in slightly closer $reca_l$ of 88.78% and 91.62%, correspondingly. In addition, the ETC technique realizes moderate $reca_l$ of 93.46%. Additionally, the RF technique reaches reasonable $reca_l$ of 97.10%. However, the IWEIC-GOADL technique outcomes in higher $reca_l$ of 99.13%.

Fig. 13 reveals a comparative analysis of the IWEIC-GOADL method with recent models concerning F_{score}. The outcomes implied that the LR algorithm determines a lower F_{score} of 88.36%. Likewise, the SVM and DTC approach outcomes in somewhat closer F_{score} of 88.77% and 91.06%, respectively. Meanwhile, the ETC approach realizes moderate F_{score} of 92.80%. Furthermore, the RF approach gains reasonable F_{score} of 97.23%. Finally, the IWEIC-GOADL methodology outcomes in enhanced F_{score} of 99.16%. Therefore, these results assured the betterment of the IWEIC-GOADL technique.
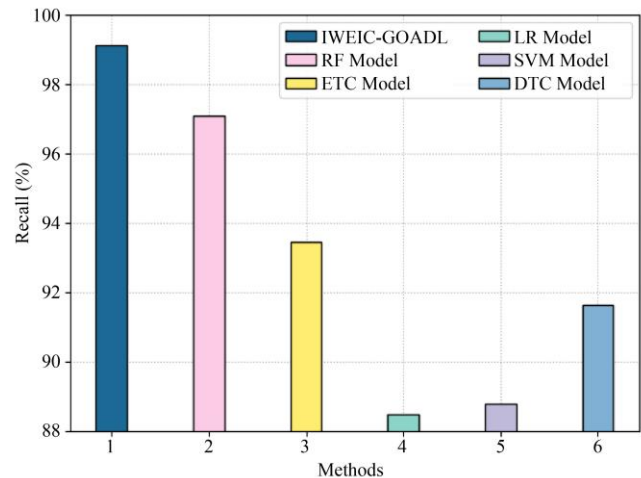
Fig. 12 $Reca_l$ analysis of the IWEIC-GOADL algorithm with other existing systems
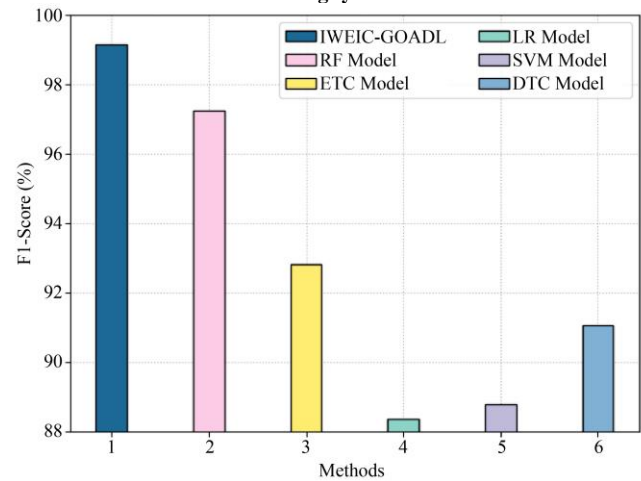
Fig. 13 $F1_{score}$ analysis of the IWEIC-GOADL algorithm with other existing systems

5. Conclusion

In this research, a novel IWEIC-GOADL procedure has been introduced for WCE image categorization. The presented IWEIC-GOADL technique encompasses a GOA-based hyperparameter optimizer, GF preprocessing, DeVGG19 feature extraction, and DBN-based classification. In the presented IWEIC-GOADL technique, the GOA is applied as a hyperparameter optimizer, enhancing the overall performance of the WCI classification. To depict the better accomplishment of the IWEIC-GODL technique, a wide range of duplications were accomplished on the benchmark dataset. The stimulation outcomes stated the improvements of the IWEIC-GODL algorithm over other recent techniques.

References

[1] Amna Liaqat et al., "Gastric Tract Infections Detection and Classification From Wireless Capsule Endoscopy Using Computer Vision Techniques : AReview," *Current Medical Imaging*, vol. 16, no. 10, pp.1229-1242, 2020. [CrossRef] [Google Scholar] [Publisher Link]

[2] Tariq Rahim, Muhammad Arslan Usman, and Soo Young Shin " A Survey on Contemporary Computer-Aided Tumor, Polyp, and Ulcer Detection Methods in Wireless Capsule Endoscopy Imaging," *Computerized Medical Imaging and Graphics*, vol. 85, p. 101767, 2020. [CrossRef] [Google Scholar] [Publisher Link]

[3] Muhammad Attique Khan et al., "Computer-Aided Gastrointestinal Diseases Analysis From Wireless Capsule Endoscopy: A Framework of Best Features Selection," *IEEE Access*, vol. 8, pp.132850-132859, 2020. [CrossRef] [Google Scholar] [Publisher Link]

[4] Khan Muhammad et al., "Vision-Based Personalized Wireless Capsule Endoscopy for Smart Healthcare: Taxonomy, Literature Review, Opportunities and Challenges," *Future Generation Computer Systems*, vol. 113, pp. 266-280, 2020. [CrossRef] [Google Scholar] [Publisher Link]

[5] R. Surendiran et al., "Exploring the Cervical Cancer Prediction By Machine Learning and Deep Learning with Artificial Intelligence Approaches," *International Journal of Engineering Trends and Technology*, vol. 70, no.7, pp.94-107, 2022. [CrossRef] [Publisher Link]

[6] Zhiguo Xiao, and Li Nian Feng, "A Study on Wireless Capsule Endoscopy for Small Intestinal Lesions Detection Based on Deep Learning Target Detection," *IEEE Access*, vol. 8, pp.159017-159026, 2020. [CrossRef] [Google Scholar] [Publisher Link]

[7] Michael Vasilakakis, Georgia Sovatzidi, and Dimitris K. Iakovidis, "Explainable Classification of Weakly Annotated Wireless Capsule Endoscopy Images Based on A Fuzzy Bag-of-Colour Features Model and Brain Storm Optimization," *International Conference on Medical Image Computing and Computer-Assisted Intervention*, Springer, Cham, vol. 12903, 2021. [CrossRef] [Google Scholar] [Publisher Link]

[8] Hiroaki Saito MD et al., " Automatic Detection and Classification of Protruding Lesions in Wireless Capsule Endoscopy Images Based on A Deep Convolutional Neural Network," *Gastrointestinal Endoscopy*, vol. 92, no. 1, pp.144-151, 2020. [CrossRef] [Google Scholar] [Publisher Link]

[9] Yan Gao et al., "Deep Model-Based Semi-Supervised Learning Way for Outlier Detection in Wireless Capsule Endoscopy Images," *IEEE Access*, vol. 8, pp. 81621-81632, 2020. [CrossRef] [Google Scholar] [Publisher Link]

[10] Vrushali Raut et al., "Gastrointestinal Tract Disease Segmentation and Classification in Wireless Capsule Endoscopy Using Intelligent Deep Learning Mode," *Computer Methods in Biomechanics and Biomedical Engineering: Imaging & Visualization*, pp.1-17, 2022. [CrossRef] [Google Scholar] [Publisher Link]

[11]   B. Sai Bharadwaj, and Ch.Sumanth Kumar, "A Novel Digital Phonocardiography Method to Identify the Cardiac Sounds Through Intrinsic Time Scale Decomposition and Inter Time Space Measurement Between Cardiac Sounds," *SSRG International Journal of Electrical and Electronics Engineering*, vol. 9, no. 12, pp. 22-29, 2022. [CrossRef] [Publisher Link]

[12] T. Madhubala, R. Umagandhi, and P. Sathiamurthi, "Diabetes Prediction Using Improved Artificial Neural Network Using Multilayer Perceptron," *SSRG International Journal of Electrical and Electronics Engineering*, vol. 9, no. 12, pp. 167-179, 2022. [CrossRef] [Publisher Link]

[13] V. Banupriya, and S. Anusuya, "Improving Classification of Retinal Fundus Image Using Flow Dynamics Optimized Deep Learning Methods," *SSRG International Journal of Electrical and Electronics Engineering*, vol. 9, no. 12, pp. 39-48, 2022. [CrossRef] [Publisher Link]

[14] S. Aiswarya et al., "Latency Reduction in Medical Iot Using Fuzzy Systems By Enabling Optimized Fog Computing," *SSRG International Journal of Electrical and Electronics Engineering*, vol. 9, no. 12, pp. 156-166, 2022. [CrossRef] [Publisher Link]

[15] Soumya Gadag, and P. Pradeepa, "A Critical Literature Review on Computer Vision Based Melanoma Detection and Identification," *SSRG International Journal of Electrical and Electronics Engineering*, vol. 9, no. 12, pp. 59-80, 2022. [CrossRef] [Publisher Link]

[16] Ayoub Ellahyani et al., "Detection of Abnormalities in Wireless Capsule Endoscopy Based on Extreme Learning Machine," *Signal, Image and Video Processing*, vol. 15, no. 5, pp.877-884, 2021. [CrossRef] [Google Scholar] [Publisher Link]

[17] Haya Alaskar et al., "Application of Convolutional Neural Networks for Automated Ulcer Detection in Wireless Capsule Endoscopy Images," *Sensors*, vol. 19, no. 6, p.1265, 2019. [CrossRef] [Google Scholar] [Publisher Link]

[18] S. Bhuvaneswari et al., "Disease Detection in Plant Leaf Using Lnet Based on Deep Learning," *International Journal of Engineering Trends and Technology*, vol. 70, no. 9, pp.64-75, 2022. [CrossRef] [Publisher Link]

[19] Diego Marin-Santos et al., "Automatic Detection of Crohn Disease in Wireless Capsule Endoscopic Images Using A Deep Convolutional Neural Network," *Applied Intelligence*, pp.1-15, 2022. [CrossRef] [Google Scholar] [Publisher Link]

[20] Samir Jain et al., "A Deep CNN Model for Anomaly Detection and Localization in Wireless Capsule Endoscopy Images," *Computers in Biology and Medicine*, vol. 137, p. 104789, 2021. [CrossRef] [Google Scholar] [Publisher Link]

[21] Gargi Sharma, and Gourav Shrivastava, "Crop Disease Prediction Using Deep Learning Techniques - A Review," *SSRG International Journal of Computer Science and Engineering* , vol. 9, no. 4, pp. 23-28, 2022. [CrossRef] [Publisher Link]

[22] Amani Abdulrahman Albraikan et al., "Modified Barnacles Mating Optimization with Deep Learning Based Weed Detection Model for Smart Agriculture," *Applied Sciences*, vol. 12, no. 24, p.12828, p. 2022.[CrossRef] [Google Scholar] [Publisher Link]

[23] Shengqi Guan, Ming Lei, and Hao Lu, "A Steel Surface Defect Recognition Algorithm Based on Improved Deep Learning Network Model Using Feature Visualization and Quality Evaluation," *IEEE Access*, vol. 8, pp.49885-49895, 2020.[CrossRef] [Google Scholar] [Publisher Link]

[24] Dr.V.V.Narendra Kumar, and T.Satish Kumar, "Smarter Artificial Intelligence with Deep Learning," *SSRG International Journal of Computer Science and Engineering* , vol. 5, no. 6, pp. 10-16, 2018. [CrossRef] [Publisher Link]

[25] Manal Abdullah Alohali et al., "Artificial Intelligence Enabled Intrusion Detection Systems for Cognitive Cyber-Physical Systems in Industry 4.0 Environment, " *Cognitive Neurodynamics*, vol. 16, no. 5, pp.1045-1057, 2022. [CrossRef] [Google Scholar] [Publisher Link]

[26] R. Surendiran et al., " A Systematic Review Using Machine Learning Algorithms for Predicting Preterm Birth," *International Journal of Engineering Trends and Technology*, vol. 70, no. 5, pp.46-59, 2022. [CrossRef] [Publisher Link]

[27] Vani, V., and Prashanth, K.M, "Ulcer Detection in Wireless Capsule Endoscopy Images Using Deep CNN," *Journal of King Saud University-Computer and Information Sciences*, vol. 34, no. 6, pp. 3319-3331, 2022. [CrossRef] [Google Scholar] [Publisher Link]

[28] Jeng-Shyang Pan et al., "A Parallel Compact Gannet Optimization Algorithm for Solving Engineering Optimization Problems," *Mathematics*, vol. 11, no. 2, p. 439, 2023. [CrossRef] [Google Scholar] [Publisher Link]

[29] P. Muruganantham, and S.M. Balakrishnan, "A Survey on Deep Learning Models for Wireless Capsule Endoscopy Image Analysis," *International Journal of Cognitive Computing in Engineering*, vol. 2, pp.83-92, 2021. [CrossRef] [Google Scholar] [Publisher Link]

[30] Geonhui Son et al., "Small Bowel Detection for Wireless Capsule Endoscopy Using Convolutional Neural Networks with Temporal Filtering," *Diagnostics*, vol. 12, no. 8, p.1858, 2022. [CrossRef] [Google Scholar] [Publisher Link]